ACS PHYSICAL CHEMISTRY Au
AN OPEN ACCESS JOURNAL OF THE AMERICAN CHEMICAL SOCIETY

pubs.acs.org/physchemau
Article

p-Sulfonatocalix[6]arene-Functionalized Gold Nanoparticles: Applications in Drug Delivery and Bioimaging

Suprotim Koley, Paacha Kandy Risla Sherin, Minati Nayak, Nilotpal Barooah, Achikanath C. Bhasikuttan,* and Jyotirmayee Mohanty*

Cite This: *ACS Phys. Chem Au* 2024, 4, 522−530
Read Online

ACCESS | Metrics & More | Article Recommendations | Supporting Information

ABSTRACT: Surface-functionalized noble metal nanoparticles with macrocyclic hosts have attracted enormous research interest owing to their applications in drug delivery, catalysis, bioimaging, etc. Stable *p*-sulfonatocalix[6]arene-functionalized gold nanoparticles (SCx6AuNPs) of the sizes ∼7.5 nm have been synthesized and characterized by using UV−vis absorption, transmission electron microscopy, and surface-enhanced Raman spectroscopy measurements. The efficient uptake and stimuli-responsive release of doxorubicin (Dox), an anticancer drug, by the SCx6AuNPs have been established for targeted drug delivery application. The decreased cytotoxicity of Dox loaded on SCx6AuNPs, especially toward normal cell lines, and its multi-stimuli responsive release validated in both cancerous (A549) and normal (W126) cell lines find promising for selectively targeted drug delivery applications toward cancer cells. At the cellular level, this study also establishes the efficient uptake of the SCx6AuNP nanoconjugates, and its validation has been done by bioimaging measurement by using thioflavin T (ThT) dye loaded on to SCx6AuNPs instead of Dox as the fluorescent tracking probe. The bright fluorescence microscopic image of ThT-SCx6AuNP-stained cancerous cell lines corroborates the uptake of SCx6AuNPs by the cell lines and its projected utility for drug delivery and bioimaging applications.

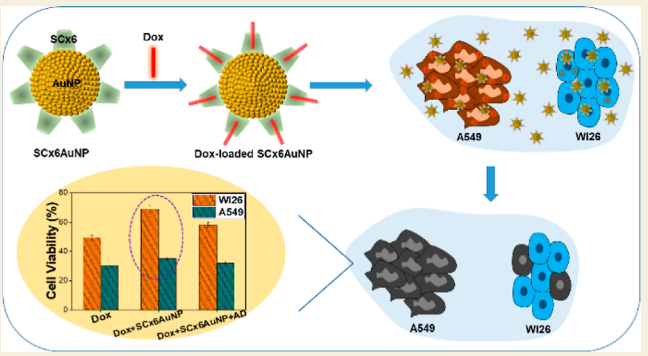

KEYWORDS: *p-sulfonatocalix[6]arene, functionalized gold nanoparticles, host−guest complexation, drug delivery, bioimaging*

INTRODUCTION

Gold nanoparticles (AuNPs) have attracted significant attention as exceptionally effective nanocarriers for treating severe diseases, such as cancer, owing to their outstanding biocompatibility, targeted drug delivery capabilities, and the potential to minimize side effects.[1−3] The UV−vis absorption spectra of AuNPs, characterized by the localized surface plasmon resonance (LSPR) band, can be harnessed for sensing applications.[4−6] Moreover, the ease of synthesis and the opportunity to modify the surface of gold nanoparticles further enhance their attractiveness for a wide range of applications.[7,8] Despite various methods (ball milling, sol−gel, chemical reduction, etc.) and stabilizing agents employed in the synthesis of gold nanoparticles, there remains a pressing need to enhance their water solubility, achieve targeted drug release, and improve overall stability.[9,10] Among many strategies, macrocyclic host (cucurbituril, cyclodextrin, calixarene, and pillararene)-capped nanoparticles have revealed significant advantages over conventional capping agents because of several factors.[11,12] Capping with water-soluble host molecules, such as *p*-sulfonatocalix[*n*]arene, cucurbiturils, sulfonated cyclodextrins, etc., can increase the solubility of nanoparticles, making them more biocompatible. The hydrophobic cavity of hosts present in these nanoparticles plays a pivotal role, allowing for the loading of crucial molecules such as therapeutic and diagnostic agents on to the host molecules functionalized on the nanoparticle surface through noncovalent interactions, mainly electrostatic, hydrophobic, H-bonding, $\pi-\pi$ stacking, etc.[13,14] Taking advantage of the reversibility of such relatively weak supramolecular interactions, stimuli responsive release of drug molecules at the preferred site can be achieved conveniently by tuning pH, temperature, ionic strength, etc.[15−17] Such approaches are used to achieve reduced degradation of therapeutic agents at physiological pH, thereby increasing the bioavailability of molecules through enhanced systemic circulation. This helps in minimizing the dose of important drug molecules with high side effects.

Calixarenes represent an essential class of host molecules recognized for their antibacterial activity against specific

Received: April 8, 2024
Revised: July 10, 2024
Accepted: July 11, 2024
Published: July 22, 2024

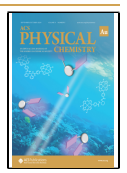

bacteria and their ability to interact with and modulate the functions of biologically important molecules.[18−21] *p*-sulfonatocalix[6]arene (SCx6, Chart 1), a water-soluble

Chart 1. Chemical Structures of SCx6, Dox, and ThT

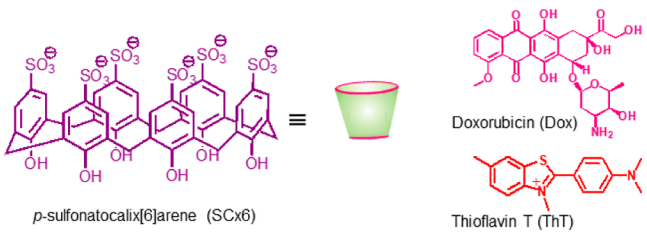

derivative of calixarene, can serve as a capping agent, thereby enhancing the water solubility and biocompatibility of nanoparticles.[21] In one of our earlier studies, the inhibition of fibril formation and disintegration of amyloid fibrils in the presence of calixarenes have been achieved.[22] SCx6 contains sulfonato groups at the upper rim with negative charge density, which further contributes to their preferential binding with cationic guests/metal ions.[23−25] Moreover, binding/uptake of small dye/drug molecules by the macrocycles modulates the physicochemical properties of the guest dye/drug, which can be tuned for customized stimuli responsive applications.[26−28]

Doxorubicin (Dox, Chart 1), a class of anthracycline antibiotic, is widely used now-a-days for cancer therapy.[29,30] Although, it is one of the most popular chemotherapeutic agents for cancer treatments, severe side effects (nausea, vomiting, hair loss, cardiotoxicity) are a major concern with this drug molecule.[31,32] A given dose of Dox administered to a patient affects both normal and cancerous cells. Therefore, opting for an improved drug delivery system utilizing gold nanoparticles as a platform for targeted drug release presents an appealing choice to address these challenges.

In this regard, considering the advantageous chemical features of the *p*-sulfonatocalix[6]arene (SCx6) host and the AuNPs, we planned to work on a stimuli-responsive nanoconjugate system based on SCx6 and AuNPs (SCx6AuNPs) for the enhancement of the drug activity and mitigation of cytotoxicity of Dox and bioimaging applications. In the SCx6AuNPs conjugate, since the SCx6 host molecules are attached to the surface of the AuNPs, one of the portals of SCx6 would remain free to interact with the dye/drug molecules and could be the site for stimuli responsive binding and release mechanisms. On the other hand, uptake of drugs/fluorescent probes by the cellular components is an essential requirement for drug delivery and cellular imaging so that various biological mechanisms and processes can be monitored and evaluated.[33−35] Fluorescence-based techniques offer significant advantages over radiation imaging, primarily due to their lower impact on cell lines and tissues. In the present case, though Dox is an emissive dye/drug, its interaction with nanoparticles, in general, leads to the quenching of their emissive states and renders them nonemissive. Therefore, to validate/confirm the uptake of Dox-loaded SCx6AuNPs by the cell lines, we introduce thioflavin T (ThT) as a tracking dye loaded onto SCx6AuNPs as the imaging probe to track the presence of the nanoconjugates in the cellular medium. ThT is a cationic dye that is commonly used to detect the formation of amyloid fibrils in tissues, which is associated with chronic diseases such as Alzheimer's and Parkinson's.[36,37] ThT specifically binds to protein fibrils, and its fluorescence increases significantly upon binding to the cavities in the amyloid fibrils, making it a highly sensitive and versatile tool for detecting amyloid fibrils in tissues.[38,39] Similarly, ThT encapsulated in macrocyclic host molecules, such as SCx6, gets its fluorescence quantum yield enhanced many fold and hence can be a convenient tracking dye, loaded to SCx6AuNPs, for cellular imaging purposes.

In this study, we synthesize and characterize SCx6-capped gold nanoparticles (SCx6AuNPs) and validate that the photostability and various other physical properties of SCx-capped gold nanoparticles are much superior as compared to those of the uncapped AuNPs. The characterized SCx6-functionalized AuNPs have been deployed to take up the drug Dox and have been characterized by various spectroscopic means. The release of Dox from the SCx6AuNPs has been evidently documented in response to external stimuli such as pH, temperature, etc., and the mechanism has been validated using the data on cell viability of Dox-loaded SCx6AuNPs nanoparticles in normal and cancerous cell lines. This study also reports on the cellular imaging measurements carried out on A549 cell lines with ThT-loaded SCx6AuNPs, bringing out bright cellular images and thereby confirming the cellular uptake of the nanoconjugate, making ways for the uptake and release of SCx6-binding potential drugs/probes.

EXPERIMENTAL SECTION

Materials

Gold(III) chloride trihydrate (99.9%), sodium borohydride (>98%), Dox hydrochloride, ThT, amantadine hydrochloride (AD), and spermidine trihydrochloride all were purchased from Sigma-Aldrich and used as received. *p*-Sulfonatocalix[6]arene was obtained from Alfa Aesar.

Instruments

Absorption spectra were recorded with a Shimadzu (UV-3600 Plus) UV−VIS−NIR spectrophotometer (Tokyo, Japan). Steady-state fluorescence spectra were recorded using an FS5 spectrofluorometer (Edinburgh Instruments, UK). TEM measurements were carried out using a field emission gun transmission electron microscope (FEI TECNAI G2, F30, 200 keV) at SAIF, IIT Bombay, India. Surface enhanced Raman spectroscopy (SERS) measurements of SCx6-coated AuNPs and bare AuNPs in aqueous solution were carried out by recording the spectra at room temperature using a 532 nm laser source from a diode-pumped solid state (DPSS) Nd^{3+}:YAG laser (Cobolt Samba 0532-01-0500-500) M/s Cobolt AB, Sweden. The sample was taken in a standard 1 × 1 cm^2 cuvette, and the scattered light was collected at 90° scattering geometry and the signal detected using a charge-coupled device (CCD, Synapse, HORIBA Jobin Yvon)-based monochromator (Triax550/LabRAM HR800, HORIBA Jobin Yvon, France) together with edge filters for 532 and 633 nm. Atomic force microscopic (AFM) images of gold nanoparticles with and without SCx6 were recorded in semicontact mode using a NT-MDT solver model instrument with a 50 μm scanner head and silicon nitride tip.

Cytotoxicity Studies

The MTT assay was carried out for the evaluation of the cytotoxicity of synthesized SCx6AuNPs, Dox, Dox-loaded SCx6AuNPs, and other multicomponent systems in both the human diploid fibroblast cell line (WI26) and the human lung carcinoma A549 cell line. The two types of cells were grown as monolayers in phenol red-free Dulbecco's modified Eagle's medium (DMEM), supplemented with 10% fetal bovine serum, 100 μg/mL streptomycin, and 100 U/mL penicillin, within a controlled environment at 37 °C, 5% CO_2, and with humidified air. Briefly, approximately 2 × 10^4 cells suspended in 200 μL of phenol-free DMEM medium were seeded into each well of a 96-

https://doi.org/10.1021/acsphyschemau.4c00027
ACS Phys. Chem Au 2024, 4, 522−530

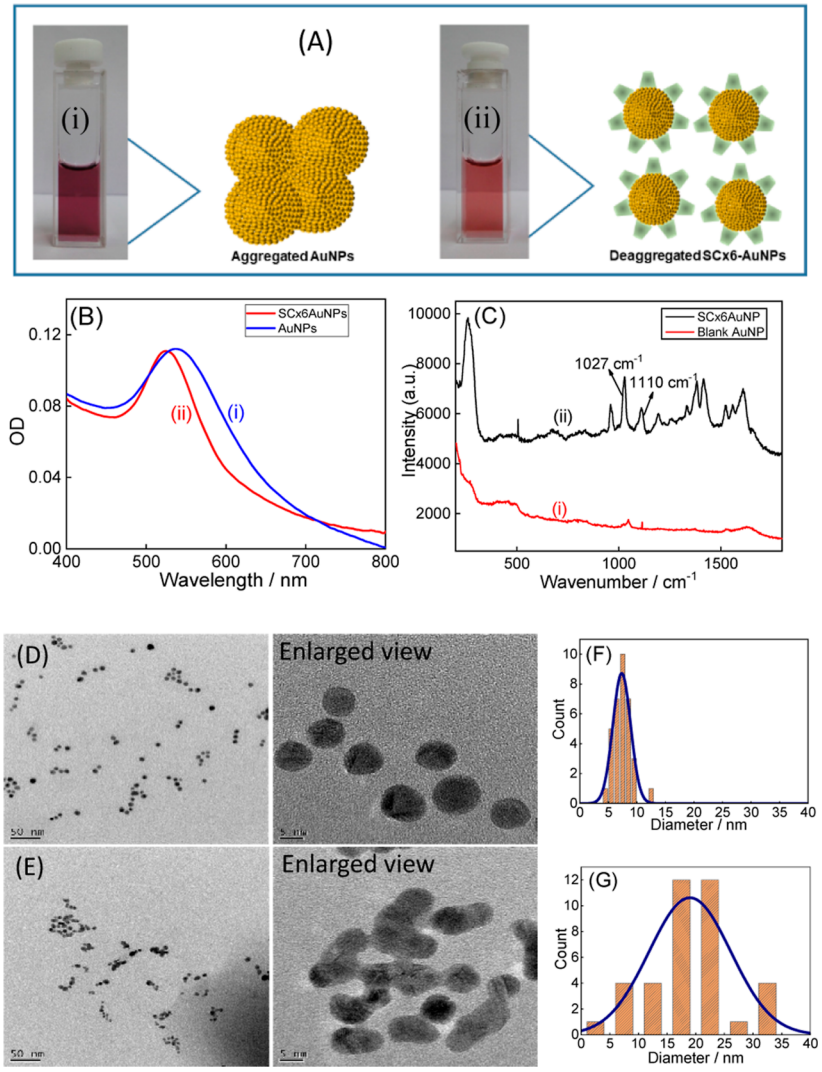

Figure 1. Synthesized gold nanoparticles in the absence (i) and presence (ii) of SCx6 (A), UV−vis absorption spectra, (B) and SERS spectra (C) of blank AuNPs (i) and SCx6AuNPs (ii); TEM images (D,E) and size distributions (F,G) of SCx6AuNPs and blank AuNPs, respectively.

well plate. The cells were then treated with the desired concentrations of samples and incubated at 37 °C for 2 h. Following this, cells were cultured for 48 h in the humidified incubator and processed for the MTT assay as described previously.[40] The control group comprises cells cultivated in DMEM medium without any intervention. Cell viability percentage was determined by assessing the reduction in absorbance at 570 nm among the treated groups relative to the control group. The experiment was done in triplicate (n = 3). The statistical significance of the variability among the means of treatment groups was determined by a t-test, and $P < 0.05$ was considered significant.

RESULTS AND DISCUSSION

Synthesis and Characterization of SCx6-Functionalized Gold Nanoparticles

Nanoparticles were prepared by a wet chemical reduction method at room temperature. About 0.25 mL of 10 mM $HAuCl_4$ solution was added to 1.5 mL of 10 mM SCx6 solution and stirred for 15 min. Next, the solution was diluted with the addition of 6 mL of water. To this, 0.6 mL of 10 mM $NaBH_4$ was added in a dropwise manner. The solution changed from yellow to reddish, indicating the formation of gold nanoparticles. After 30 min of stirring, the absorption spectrum of the solution was taken. The surface plasmon band became narrower and shifted to 525 nm as compared to the relatively broader band of bare AuNP at 538 nm, confirming the formation of SCx6-functionalized AuNPs, Figure 1A(i,ii).[41] The formed Au nanoparticles were centrifuged at 10,000 rpm for 10 min and washed with water to remove excess $NaBH_4$ and SCx6. Then, the nanoparticles were redispersed in water by sonication, and further photophysical studies were carried out. The nanoparticles were characterized by UV−vis absorption, SERS, TEM, and AFM measurements. The concentration of free and capped AuNPs has been evaluated by considering its extinction coefficient as 5.14×10^7 M^{-1} cm^{-1}, reported before.[42]

The SERS spectrum of SCx6-capped AuNPs exhibits characteristic peak shifts in the normal modes of SO_3^- groups (Figure 1C), 1170 cm^{-1} in SCx6 to 1110 cm^{-1} in SCx6AuNP and 1044 cm^{-1} in SCx6 to 1027 cm^{-1} in SCx6AuNP. Weakening of these bonds evidently indicates that the SCx6 attachment on the AuNP surface is through SO_3^- groups of SCx6.[13,43] For uncapped AuNPs, no such characteristic peaks are observed in SERS (Figure 1C). TEM measurements show the morphologies (Figure 1D,E) and size distributions of both kinds of nanoparticles (Figure 1F,G). SCx6AuNPs display

https://doi.org/10.1021/acsphyschemau.4c00027
ACS Phys. Chem Au 2024, 4, 522−530

spherical shapes with smaller sizes and a monodispersed size distribution, characterized by a mean diameter of approximately 7.5 nm. In the case of uncapped nanoparticles, large agglomeration is observed with a polydispersed size distribution with a mean diameter of around 19 nm. All these morphologies are further supported by AFM measurements (Figure S1, Supporting Information).

Nanoparticles, owing to their smaller sizes, have a large surface area/volume ratio, resulting in excess surface energy in the system.[44] For any practical application, inhibition of this agglomeration is a primary requirement. The change in optical density (OD) at the respective peak positions of both nanoparticles was recorded over a period of time to monitor their agglomeration behavior. As shown in Figure 2, the extent

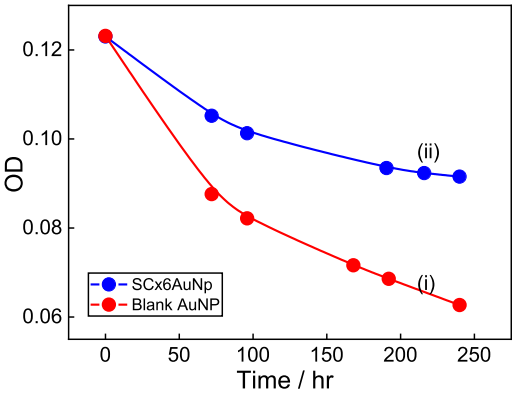

Figure 2. Change in OD of AuNP (i) and SCx6AuNP (ii) with time at ambient conditions.

of the decrease in OD over a certain time period for uncapped AuNPs is much higher compared to SCx6-capped AuNPs. The presence of −ve charge ($-SO_3^-$ group) on SCx6 causes repulsions between AuNPs, which hinders the unwanted agglomeration of SCx6-capped nanoparticles. The small decrease (∼25%) in OD as well as no change in the peak position of the LSPR band in SCx6-capped AuNPs, even after 2 months of preparation, is attributed to the minor agglomeration of these nanoparticles. However, in the case of blank AuNPs, the OD decreases markedly (∼50%) along with the change in the shape and peak position of the LSPR band. The substantial increase in the stability of AuNPs after capping significantly enhances their applicability as drug nanocarriers.

Ground-State Absorption and Fluorescence Studies of Dox and SCx6AuNPs

All photophysical studies were carried out in Tris buffer (10 mM) at pH 7.5 to emulate physiological conditions. Dox shows a broad absorption spectrum in the wavelength range of 400−550 nm, having two closely spaced peaks at 480 and 495 nm at pH 7.5. The addition of SCx6AuNPs to the solution of Dox causes an increase in the OD of the system due to the overlapping of the LSPR band in this region. As a result, many insights were not obtained from this overlapping absorption spectrum (Figure 3A).

The fluorescence study of Dox upon the addition of SCx6AuNPs was performed to observe the changes in its emission behavior. Dox shows moderate fluorescence emission (λ_{ex} = 480 nm) in the wavelength range of 520−750 nm at pH 7.5. Gradual addition of SCx6AuNPs to Dox causes rapid quenching of the fluorescence intensity of Dox, indicating efficient interaction/uptake of Dox by the SCx6AuNPs. The quenching is attributed to the formation of a noncovalent host−guest complex between SCx6 present on the nanoparticle surface and Dox. From the changes in emission with the increasing concentration of SCx6AuNPs, the binding isotherm is constructed (inset, Figure 3B), and the binding constant value was evaluated as $(1.1 \pm 0.1) \times 10^9$ M^{-1} by assuming a 1:1 stoichiometry and fitting the isotherm with the modified Benesi−Hildebrand binding model (Note S1, Supporting Information).[45] The 1:1 stoichiometry assumption for the interaction of Dox with SCx6AuNP was based on the 1:1 stoichiometry evaluated for the SCx6 host, which is the encapsulating unit, with Dox (Figure S2, Supporting Information). Since the number of SCx6 on the surface of the SCx6AuNP is not known, the interaction of SCx6AuNPs with Dox was also assumed to follow a 1:1 stoichiometry. The nanomolar concentration of SCx6AuNPs was sufficient to achieve substantial quenching of the Dox emission, which suggests a strong interaction between nanoparticles and Dox. The high binding constant value indicates that the interaction is mainly driven by the electrostatic interaction between the phenolate groups of SCx6 attached to the surface of AuNPs and the amine group of Dox at pH 7.5. There could be some possibility of a $\pi-\pi$ interaction between SCx6 and Dox. At the saturated concentration of SCx6AuNPs, the concentration of SCx6 was about 54 μM, which is ∼5 times less as compared to the concentration of SCx6 required (245 μM) to attain saturation during the titration of Dox with SCx6 host alone (Figure S3, Supporting Information). The enhanced binding interaction and saturation at a very low concentration of SCx6

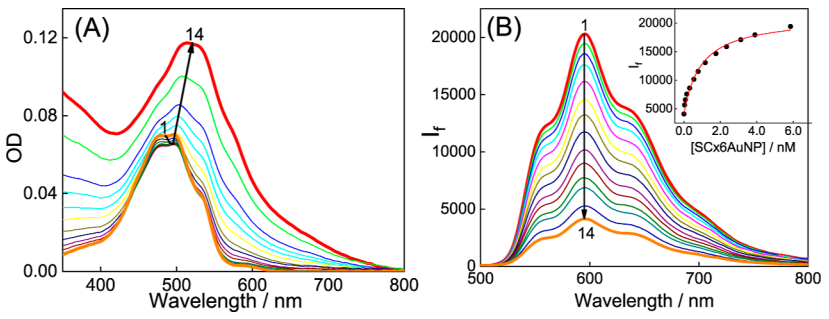

Figure 3. (A) Absorption and (B) Emission spectrum of Dox at different concentrations of SCx6AuNPs in TRIS buffer (pH 7.5). [SCx6AuNPs]/nM: (1) 0, (2) 0.04, (3) 0.08, (4) 0.16, (5) 0.31, (6) 0.55, (7) 0.78, (8) 1.17, (9) 1.75, (10) 2.34, (11) 3.12, (12) 3.9, (13) 5.85, and (14) 7.8. Inset of (B) shows the binding isotherm of Dox with SCx6AuNPs.

https://doi.org/10.1021/acsphyschemau.4c00027
ACS Phys. Chem Au 2024, 4, 522−530

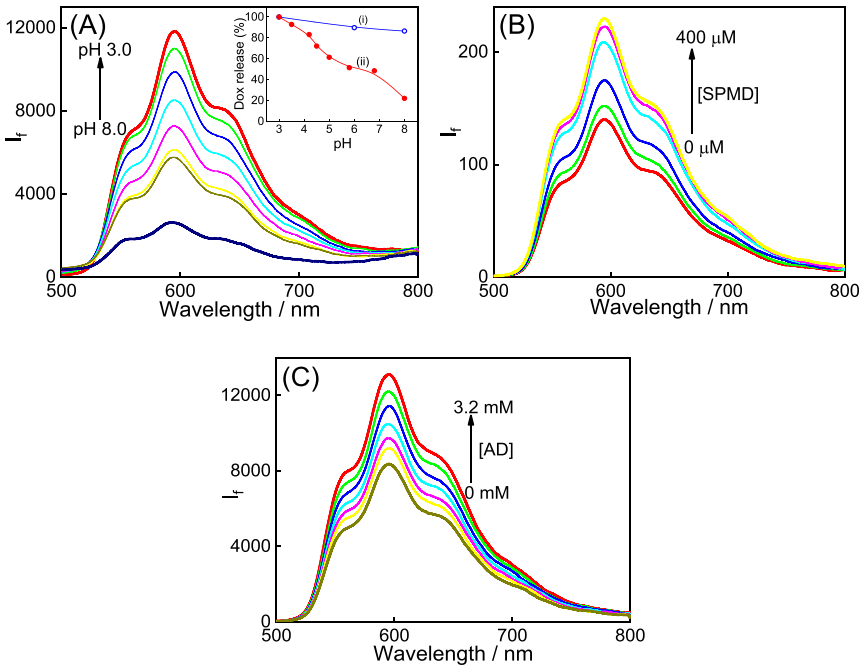

Figure 4. Stimuli-responsive release of Dox from SCx6AuNPs with (A) decreasing pH and increasing concentration of spermidine (B)/AD (C). Inset of (A) shows the release of Dox (%) with pH.

(~54 μM) in SCx6AuNPs is one of the advantages of SCx6 functionalized AuNPs over the five times higher (~245 μM) free SCx6 concentration required to attain the saturation required to form the complex with Dox. This would be highly advantageous to minimize the concentration of the SCx6 additive as a drug carrier.

The control measurement, titration between Dox and uncapped AuNPs, shows quenching in the fluorescence intensity of Dox (Figure S4, Supporting Information); however, the extent of quenching is much less as compared to the SCx6AuNPs. This result could be attributed to nanosurface energy transfer (NSET) from the Dox to AuNPs, as the fluorescence spectra of Dox overlap with the absorption spectra of AuNP (Figure S5, Supporting Information).[46] The large changes in Dox in the presence of SCx6AuNPs are due to the combination of NSET as well as the interaction between surface SCx6 and Dox. From the data on the total Dox added and the amount of Dox not interacted, the uptake efficiency was calculated to be ~79.5% in the low concentration domain. Whereas, the loading efficiency has been evaluated at 5.3% considering the gram of Dox loaded per gram of the nanoparticles and is well in the range of values reported for Dox by other systems.[47,48]

Time-resolved fluorescence measurements of Dox with and without SCx6AuNPs have been carried out using a time-correlated single-photon counting (TCSPC) setup. Dox shows two lifetime values, with a shorter component of 230 ps having a 10% contribution and a long component of ~960 ps and an average lifetime of 870 ps. However, no significant change in the excited state lifetime is observed upon addition of SCx6AuNPs to the Dox solution (S6A, Supporting Information), and the average lifetime remains the same (Figure S6B and Table S1, Supporting Information). This indicates the static nature of the fluorescence quenching, where the ground-state complex formed between Dox and SCx6AuNPs itself is nonfluorescent. In combination with the above discussion on NSET, the overall extent of quenching of Dox in the presence of SCx6AuNP can be assigned to the combination of NSET and ground state complex formation.

Stimuli-Responsive Release of Dox from SCx6AuNPs

From the binding constant values, it is inferred that the host–guest complex of SCx6AuNPs with Dox is highly stable at the physiological pH of 7.5, which is a prerequisite to avoid the leakage of the drug at nontarget sites. Once the drug has reached the target site, release of the drug can be triggered in response to specific external stimuli. The release of Dox from SCx6AuNPs has been monitored by observing the restoration of Dox fluorescence in the presence of external stimuli such as pH of the solution, addition of competitive binder, i.e., spermidine (SPMD), AD (also known as an antiviral and anti-Parkinson drug), and temperature.[49]

It is well established that cancerous cells are more acidic (pH 5–6.5) compared to healthy cells (pH 7.4) in the body.[50] Acid-responsive drug delivery systems are widely favored because they facilitate the release of drug molecules, specifically in acidic cancerous cells, thereby reducing probable side effects. The release of Dox from SCx6AuNPs has been studied by changing the pH of the solution. The increase in both the OD (Figure S7, Supporting Information) and fluorescence intensity of Dox (Figure 4B) by decreasing the pH of the solution from pH 8 to pH 3 clearly indicates the gradual release of Dox from the nanoparticle. The cumulative Dox release at pH 5 and pH 7.5 for ~48 h has been investigated by monitoring the fluorescence intensity of Dox-loaded SCx6AuNPs with time (Figure S8). It was seen that the drug release rate and yield of Dox are higher at pH 5 than those at pH 7.5 (Figure S8C). Since the pK_a of Dox is ~4.5, at lower pH, Dox remains in the cationic form, and the phenolic groups in SCx6 attached to the nanoparticle surface are in the phenol form. As a result, the electrostatic interaction between Dox and SCx6AuNP decreases and facilitates the release of Dox into the solution.

https://doi.org/10.1021/acsphyschemau.4c00027
ACS Phys. Chem Au 2024, 4, 522–530

Additionally, the release of Dox in the presence of competitive binder such as spermidine (an example of polyamine) and AD has been investigated by monitoring the fluorescence intensity of Dox (Figure 4C,D). It has been observed that the fluorescence intensity increases and attains saturation at ∼300 μM concentrations of SPMD or ∼3 mM concentrations of AD. This study indicates that the micromolar concentration of SPMD is sufficient to release the Dox completely at the target site. Because specific polyamines such as spermine and spermidine are known to be overexpressed in various cancerous cell lines, including breast and lung cancer cell lines.[51] By exploiting polyamine responsiveness, drug delivery systems can be designed for targeted drug release to cancerous cells. Therefore, it is expected that the binding of SCx6AuNPs to Dox will attenuate its therapeutic effect in normal cells. Simultaneously, the selective release of Dox from SCx6AuNPs into cancerous cells, facilitated by the acidic pH and overexpression of polyamines, is expected to significantly mitigate Dox side effects.

We have also investigated the temperature-responsive behavior of the SCx6AuNP/Dox complex system. It is observed that the fluorescence intensity of Dox regenerates gradually by increasing the temperature (Figure S9), indicating the controlled release of Dox. The weakening of noncovalent interactions between Dox and SCx6AuNPs at higher temperatures could be one of the reasons for the Dox release.[52]

Cell Viability Study of Dox in the Presence of SCx6 and SCx6AuNP

It is well acknowledged that the encapsulation of anticancer drugs by macrocyclic hosts mitigates the side effects of these drugs to a large extent.[53,54] Generally, metal nanoparticles functionalized with such macrocyclic hosts have been used to get the same benefits with a reduced concentration of macrocycles. To explore this, the cell viability study of Dox in the absence and presence of only SCx6 and SCx6AuNP in the normal human diploid fibroblast cell line (WI26) and lung cancerous cell line (A549) was carried out by using the MTT assay. It was observed that the viability of both cell lines treated with SCX6AuNPs did not reduce after 48 h with respect to the control (cell lines in DMEM medium), Figure 5(i). This clearly indicates that SCx6AuNP is nontoxic. As shown in Figure 5, the Dox-loaded SCx6AuNP showed higher cell viability than the free Dox in WI26 cell lines [Figure 5iii(a),ii(a)], whereas the cell viability of Dox-loaded SCx6AuNP is almost similar to that of free Dox in A549 cell lines [Figure 5iii(b),ii(b)]. This could be attributed to the lower pH and overexpression of polyamines in the A549 cell lines with respect to the WI26 cell lines, which facilitate the stimuli-responsive release of Dox, selectively targeting the cancerous cell lines without showing any side effects. Additionally, cell lines incubated with Dox-loaded SCx6AuNP were treated with AD, which showed a reduction in cell viability, explicitly in WI26 cells close to plain Dox, as shown in Figure 5iv. Further, as a control experiment, the cell viability study for SCx6 loaded with Dox has been carried out in WI26 and A549 cell lines. As presented in Figure 5v, there is less difference among the WI26 and A549 cell lines against bar no (iii) and almost similar cell viability with respect to Dox alone (ii). This result indicates the restoration of the toxicity of Dox on the introduction of AD or by changing pH, demonstrating the controlled activation of DOX toxicity triggered through AD or acidic intracellular pH/polyamine overexpression prevalent in the cancerous cell lines.

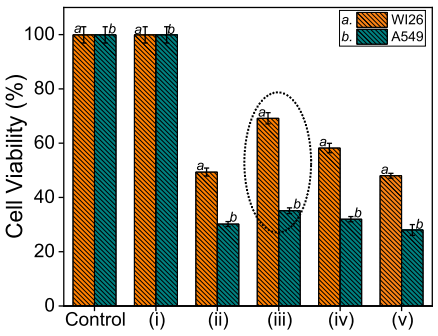

Figure 5. Cell viability in percentage using the MTT assay. (i) SCx6AuNPs, (ii) Dox (3 μM), (iii) Dox (3 μM)-loaded SCx6AuNPs, (iv) Dox (3 μM)-loaded SCx6AuNPs in the presence of AD, and (v) Dox (3 μM)-SCx6 (54 μM).

To confirm the efficient cellular uptake of the Dox loaded SCx6AuNP conjugate, fluorescence imaging studies were carried out using A549 cancer cells. However, due to the low emission yield and the severe fluorescence quenching of Dox observed on the SCx6AuNP, the imaging experiments were not successful (Figure S10). On the other hand, to demonstrate the efficient cellular uptake of the SCx6AuNP conjugate, we employed a fluorogenic dye, ThT, which turns fluorescent on encapsulation/binding to macrocycles, in place of Dox. For this, detailed interactions of ThT with SCx6AuNPs were also investigated.

ThT shows absorption in the wavelength range of 350−475 nm, with a maximum at 412 nm in Tris buffer (pH 7.5). The addition of SCx6AuNPs to ThT solution causes a red shift of ∼6 nm in the absorption maxima with the emergence of an isosbestic point at 427 nm, which indicates interaction between ThT and SCx6 capped Au nanoparticles. Along with the red shift, the absorption maximum undergoes a hypochromic shift, which can be attributed to lower polarizability of the SCx6 cavity compared to bulk water. The band developed in a higher wavelength region (500−600 nm) is due to the typical LSPR band of gold nanoparticles.

ThT exhibits weak fluorescence in an aqueous solution due to the torsional motion between the benzothiazole and dimethylaminobenzene rings.[55] The encapsulation of ThT within the SCx6 present on the surface of Au nanoparticles impedes the flexibility in the rotation of these two rings of ThT. This restriction leads to a reduction in nonradiative deexcitation processes and increases its fluorescence yield (∼10-fold). The binding isotherm (inset of Figure 6B) is constructed by plotting the fluorescence intensity at 500 nm versus the concentration of SCx6AuNP and is fitted by using the Benesi−Hildebrand equation. The binding constant value was estimated as $(1.5 \pm 0.1) \times 10^9$ M^{-1}. About 6 nM concentration of SCx6AuNP is sufficient to attain saturation, indicating a strong interaction between ThT and SCx6AuNP. Significant enhancements in the fluorescence emission of ThT loaded onto the nanoparticles hold promise for applications of ThT in cellular imaging. The lifetime of ThT is about a few picoseconds due to the highly active torsional motion, and the lifetime could not be measured using our TCSPC setup since the time-resolution of the setup is ∼50 ps. However, a slight increase in the excited state lifetime of ThT was observed with the addition of 6 nM SCx6AuNPs (Figure S11).

https://doi.org/10.1021/acsphyschemau.4c00027
ACS Phys. Chem Au 2024, 4, 522−530

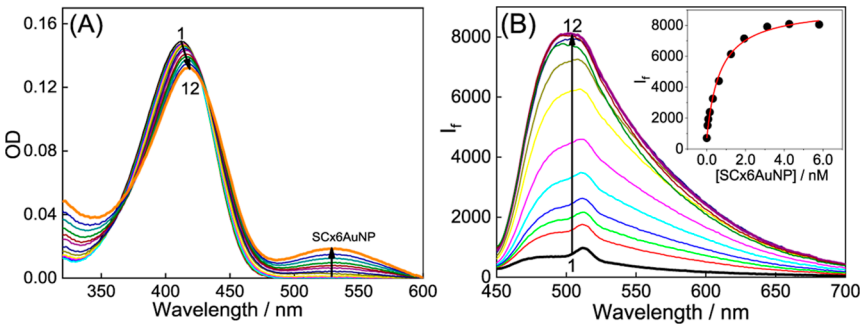

Figure 6. (A) Absorption and (B) emission spectrum of ThT at different concentrations of SCx6-AuNPs in TRIS buffer (pH 7.5). [SCx6-AuNPs]/nM: (1) 0, (2) 0.04, (3) 0.08, (4) 0.16, (5) 0.31, (6) 0.62, (7) 1.25, (8) 1.94, (9) 3.12, (10) 4.26, (11) 5.80, and (12) 7.80. Inset of (B) shows the binding isotherm of ThT with SCx6-AuNPs.

Bioimaging Study

Having confirmed that ThT-loaded SCx6AuNP can act as a fluorescent tool to track the uptake of SCx6AuNP by the cancer cells, fluorescence microscopic images were recorded using ThT or ThT-SCx6AuNPs-stained A549 cancer cells (Figure 7). As seen in the presented images, while the control

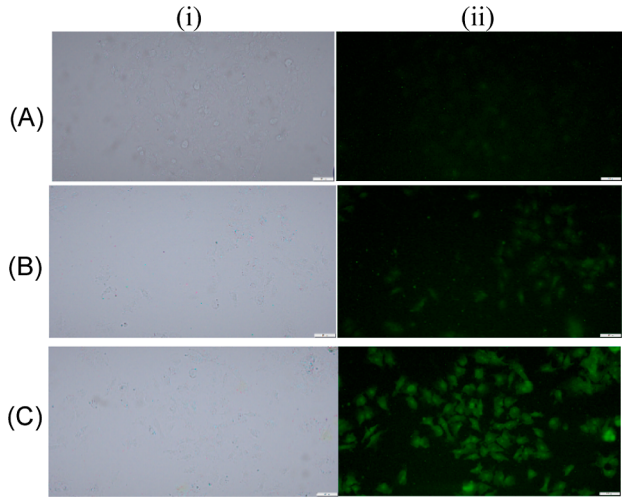

Figure 7. Bright field image (i) and fluorescence image (ii) of A549 cells; control (A), only ThT (B), and ThT- SCx6AuNPs (C).

A549 cell line without any probe did not present any image (Figure 7A), only the ThT-stained A549 cell lines presented feeble images of ThT uptake (Figure 7B). However, the ThT-loaded SCx6AuNP-stained A549 cell lines gave experimentally acceptable bright and clear cellular images (Figure 7C) for identification, confirming the uptake of SCx6AuNP nanoconjugate by the A549 cells, which can be tuned by loading them with Dox or ThT for drug delivery or imaging the cell lines. Parallelly, the toxicity of ThT and ThT-SCx6AuNPs has also been evaluated in WI26 cell lines by using the MTT assay. The cell viability of WI26 cell lines increases from blank AuNPs to SCx6AuNPs, indicating the reduced toxicity of SCx6-functionalized AuNPs. The same trend is also observed as the toxicity of ThT (~5 μM) reduced significantly upon being entrapped by SCx6AuNPs (Figure S12).

CONCLUSIONS

In this study, the interactions of *p*-sulfonatocalix[6]arene-functionalized Au nanoparticles (SCx6AuNPs) with the anticancer drug Dox as well as the fluorescence imaging dye ThT have been investigated. Stable SCx6AuNPs have been synthesized and have been characterized by various methods and are found to be of sizes ~7.5 nm, much smaller compared to the bare AuNP particles of sizes ~19 nm obtained in a similar procedure. These functionalized AuNPs have been recognized to efficiently uptake Dox as well as the fluorogenic dye ThT. The Dox-loaded SCx6AuNPs nanoconjugates have been shown to be responsive toward external stimuli such as pH, spermidine, adamantylamine, etc. as competitive binding agents. The decreased cytotoxicity of Dox loaded on the SCx6AuNPs, especially toward normal cell lines, and its multistimuli-responsive release validated in both cancerous (A549) and normal (W126) cell lines make them promising for selectively targeted drug delivery applications. By introducing ThT as the fluorescent tracking dye for bioimaging measurements, this study also establishes efficient cellular uptake of the SCx6AuNP nanoconjugates, where Dox could not be used due to its low emission features. The bright fluorescence microscopic image of ThT-SCx6AuNP stained cancerous cell lines validates the uptake of SCx6AuNPs by the cell lines and its projected utility for drug delivery applications.

ASSOCIATED CONTENT

Supporting Information

The Supporting Information is available free of charge at https://pubs.acs.org/doi/10.1021/acsphyschemau.4c00027.

AFM images, Jobs plot, additional fluorescence titration, fluorescence decay traces, fluorescence imaging, and cell viability data (PDF)

AUTHOR INFORMATION

Corresponding Authors

Achikanath C. Bhasikuttan − *Radiation & Photochemistry Division, Bhabha Atomic Research Centre, Mumbai 400085, India; Homi Bhabha National Institute, Anushaktinagar, Mumbai 400094, India;* orcid.org/0000-0001-7224-0482; Email: bkac@barc.gov.in

Jyotirmayee Mohanty − *Radiation & Photochemistry Division, Bhabha Atomic Research Centre, Mumbai 400085, India; Homi Bhabha National Institute, Anushaktinagar, Mumbai 400094, India;* orcid.org/0000-0002-2018-4906; Email: jyotim@barc.gov.in

https://doi.org/10.1021/acsphyschemau.4c00027
ACS Phys. Chem Au 2024, 4, 522−530

Authors

Suprotim Koley − *Radiation & Photochemistry Division, Bhabha Atomic Research Centre, Mumbai 400085, India*

Paacha Kandy Risla Sherin − *Radiation & Photochemistry Division, Bhabha Atomic Research Centre, Mumbai 400085, India*

Minati Nayak − *Radiation & Photochemistry Division, Bhabha Atomic Research Centre, Mumbai 400085, India; Homi Bhabha National Institute, Anushaktinagar, Mumbai 400094, India*

Nilotpal Barooah − *Radiation & Photochemistry Division, Bhabha Atomic Research Centre, Mumbai 400085, India; Homi Bhabha National Institute, Anushaktinagar, Mumbai 400094, India*

Complete contact information is available at: https://pubs.acs.org/10.1021/acsphyschemau.4c00027

Author Contributions

All authors have given approval to the final version of the manuscript. CRediT: **Jyotirmayee Mohanty** conceptualization, supervision, writing-review & editing.

Notes

The authors declare no competing financial interest.

■ ACKNOWLEDGMENTS

We thank Dr. A. Kunwar for the discussion regarding cellular experiments. J.M. acknowledges SERB, DST, for the POWER Fellowship (SPF/2022/000010). We acknowledge the help from N. Maiti for SERS measurements and V. Sudarsan for AFM measurements. We also acknowledge SAIF, IIT Bombay, India, for TEM measurements.

■ REFERENCES

(1) Bansal, S. A.; Kumar, V.; Karimi, J.; Singh, A. P.; Kumar, S. Role of gold nanoparticles in advanced biomedical applications. *Nanoscale Adv.* **2020**, *2*, 3764−3787.

(2) Lee, S.-Y.; Shieh, M.-J. Platinum (II) drug-loaded gold nanoshells for chemo-photothermal therapy in colorectal cancer. *ACS Appl. Mater. Interfaces* **2020**, *12*, 4254−4264.

(3) Mohd-Zahid, M. H.; Mohamud, R.; Abdullah, C. A. C.; Lim, J.; Alem, H.; Hanaffi, W. N. W.; Iskandar, Z. Colorectal cancer stem cells: A review of targeted drug delivery by gold nanoparticles. *RSC Adv.* **2020**, *10*, 973−985.

(4) Do, P. Q. T.; Huong, V. T.; Phuong, N. T. T.; Nguyen, T.-H.; Ta, H. K. T.; Ju, H.; Phan, T. B.; Phung, V.-D.; Tran, N. H. T.; Tran, N. H. T. The highly sensitive determination of serotonin by using gold nanoparticles (Au NPs) with a localized surface plasmon resonance (LSPR) absorption wavelength in the visible region. *RSC Adv.* **2020**, *10*, 30858−30869.

(5) Yano, T.-a.; Kajisa, T.; Ono, M.; Miyasaka, Y.; Hasegawa, Y.; Saito, A.; Otsuka, K.; Sakane, A.; Sasaki, T.; Yasutomo, K.; et al. Ultrasensitive detection of SARS-CoV-2 nucleocapsid protein using large gold nanoparticle-enhanced surface plasmon resonance. *Sci. Rep.* **2022**, *12*, 1060.

(6) Ghosh, S. K.; Pal, T. Interparticle coupling effect on the surface plasmon resonance of gold nanoparticles: from theory to applications. *Chem. Rev.* **2007**, *107*, 4797−4862.

(7) Nicol, J. R.; Dixon, D.; Coulter, J. A. Gold nanoparticle surface functionalization: A necessary requirement in the development of novel nanotherapeutics. *Nanomedicine* **2015**, *10*, 1315−1326.

(8) Lee, J. W.; Choi, S.-R.; Heo, J. H. Simultaneous stabilization and functionalization of gold nanoparticles via biomolecule conjugation: Progress and perspectives. *ACS Appl. Mater. Interfaces* **2021**, *13*, 42311−42328.

(9) Penon, O.; Patiño, T.; Barrios, L.; Nogues, C.; Amabilino, D. B.; Wurst, K.; Pérez-García, L. A New Porphyrin for the Preparation of Functionalized Water-Soluble Gold Nanoparticles with Low Intrinsic Toxicity. *ChemistryOpen* **2015**, *4*, 127−136.

(10) Guo, W.; Pleixats, R.; Shafir, A. Water-Soluble Gold Nanoparticles: From Catalytic Selective Nitroarene Reduction in Water to Refractive Index Sensing. *Chem.Asian J.* **2015**, *10* (11), 2437−2443.

(11) Lee, T. C.; Scherman, O. A. A facile synthesis of dynamic supramolecular aggregates of cucurbit [*n*] uril (*n*= 5−8) capped with gold nanoparticles in aqueous media. *Chem.—Eur. J.* **2012**, *18*, 1628−1633.

(12) Montes-García, V.; Perez-Juste, J.; Pastoriza-Santos, I.; Liz-Marzan, L. M. Metal nanoparticles and supramolecular macrocycles: a tale of synergy. In *Colloidal Synthesis of Plasmonic Nanometals*; Liz-Marzán, L., Ed.; Jenny Stanford Publishing: New York, 2020; pp 537−561.

(13) Mehra, C.; Gala, R.; Kakatkar, A.; Kumar, V.; Khurana, R.; Barooah, N.; Bhasikuttan, A. C.; Mohanty, J.; Bhasikuttan, A. C.; Mohanty, J. Cooperative enhancement of antibacterial activity of sanguinarine drug through *p*-sulfonatocalix[6]arene functionalized silver nanoparticles. *Chem. Commun.* **2019**, *55*, 14275−14278.

(14) Barooah, N.; Bhasikuttan, A. C.; Sudarsan, V.; Dutta Choudhury, S.; Pal, H.; Mohanty, J. Surface functionalized silver nanoparticle conjugates: demonstration of uptake and release of a phototherapeutic porphyrin dye. *Chem. Commun.* **2011**, *47*, 9182−9184.

(15) Shumatbaeva, A. M.; Morozova, J. E.; Syakaev, V. V.; Shalaeva, Y. V.; Sapunova, A. S.; Voloshina, A. D.; Gubaidullin, A. T.; Bazanova, O. B.; Babaev, V. M.; Nizameev, I. R.; et al. The pH-responsive calix [4] resorcinarene-mPEG conjugates bearing acylhydrazone bonds: Synthesis and study of the potential as supramolecular drug delivery systems. *Colloids Surf. A: Physicochem. Eng. Asp.* **2020**, *589*, 124453.

(16) Pennakalathil, J.; Jahja, E.; Özdemir, E. S.; Konu, O. z.; Tuncel, D. n. s. Red emitting, cucurbituril-capped, pH-responsive conjugated oligomer-based nanoparticles for drug delivery and cellular imaging. *Biomacromolecules* **2014**, *15*, 3366−3374.

(17) Wang, J.; Li, D.; Fan, Y.; Shi, M.; Yang, Y.; Wang, L.; Peng, Y.; Shen, M.; Shi, X. Core-shell tecto dendrimers formed via host-guest supramolecular assembly as pH-responsive intelligent carriers for enhanced anticancer drug delivery. *Nanoscale* **2019**, *11*, 22343−22350.

(18) Tommasone, S.; Talotta, C.; Gaeta, C.; Margarucci, L.; Monti, M. C.; Casapullo, A.; Macchi, B.; Prete, S. P.; Ladeira De Araujo, A.; Neri, P. Biomolecular fishing for calixarene partners by a chemo-proteomic approach. *Angew. Chem.* **2015**, *127*, 15625−15629.

(19) Koley, S.; Gaur, M.; Barooah, N.; Bhasikuttan, A. C.; Mohanty, J. Supramolecular assemblies with macrocyclic hosts: applications in antibacterial activity. *Pure Appl. Chem.* **2024**, *96*, 23−42.

(20) Kellici, S.; Acord, J.; Vaughn, A.; Power, N. P.; Morgan, D. J.; Heil, T.; Facq, S. P.; Lampronti, G. I. Calixarene assisted rapid synthesis of silver-graphene nanocomposites with enhanced anti-bacterial activity. *ACS Appl. Mater. Interfaces* **2016**, *8*, 19038−19046.

(21) Siddharthan, A.; Kumar, V.; Barooah, N.; Chatterjee, S.; Bhasikuttan, A. C.; Mohanty, J. Supramolecular interaction of ofloxacin drug with *p*-sulfonatocalix [6] arene: Metal-ion responsive fluorescence behavior and enhanced antibacterial activity. *J. Mol. Liq.* **2023**, *370*, 121047.

(22) Shinde, M. N.; Barooah, N.; Bhasikuttan, A. C.; Mohanty, J. Inhibition and disintegration of insulin amyloid fibrils: a facile supramolecular strategy with *p*-sulfonatocalixarenes. *Chem. Commun.* **2016**, *52*, 2992−2995.

(23) Perret, F.; Lazar, A. N.; Coleman, A. W. Biochemistry of the para-sulfonato-calix [*n*] arenes. *Chem. Commun.* **2006**, 2425−2438.

(24) Jadhav, A.; Kalyani, V. S.; Barooah, N.; Malkhede, D. D.; Mohanty, J. Molecular-Recognition-Assisted pK_a Shifts and Metal-Ion-Induced Fluorescence Regeneration in *p*-Sulfonatocalix[6]arene-Encapsulated Acridine. *ChemPhysChem* **2015**, *16*, 420−427.

(25) Shinde, M. N.; Bhasikuttan, A. C.; Mohanty, J. Recognition-mediated contrasting fluorescence behaviour of 4′,6-diamidino-2-phenylindole (DAPI): probing the pK_a of *p*-sulfonatocalix[4/6]arenes. *Supramol. Chem.* **2016**, *28*, 517−525.
(26) Shinde, M. N.; Khurana, R.; Barooah, N.; Bhasikuttan, A. C.; Mohanty, J. Metal ion-induced supramolecular pK_a tuning and fluorescence regeneration of a *p*-sulfonatocalixarene encapsulated neutral red dye. *Org. Biomol. Chem.* **2017**, *15*, 3975−3984.
(27) Kalyani, V. S.; Malkhede, D. D.; Mohanty, J. Cyclodextrin-assisted modulation of the photophysical properties and acidity constant of pyrene-armed calix[4]arene. *Phys. Chem. Chem. Phys.* **2017**, *19*, 21382−21389.
(28) Barooah, N.; Mohanty, J.; Bhasikuttan, A. C. Cucurbituril-Based Supramolecular Assemblies: Prospective on Drug Delivery, Sensing, Separation, and Catalytic Applications. *Langmuir* **2022**, *38*, 6249−6264.
(29) Arcamone, F. *Doxorubicin: Anticancer Antibiotics*; Elsevier, 2012; .
(30) Rivankar, S. An overview of doxorubicin formulations in cancer therapy. *J. Cancer Res. Ther.* **2014**, *10*, 853−858.
(31) Sritharan, S.; Sivalingam, N. A comprehensive review on time-tested anticancer drug doxorubicin. *Life Sci.* **2021**, *278*, 119527.
(32) Mobaraki, M.; Faraji, A.; Zare, M.; Dolati, P.; Ataei, M.; Manshadi, H. D. Molecular mechanisms of cardiotoxicity: a review on major side-effect of doxorubicin. *Indian J. Pharm. Sci.* **2017**, *79*, 335−344.
(33) Xu, G.-X.; Mak, E. C.-L.; Lo, K. K.-W. Photofunctional transition metal complexes as cellular probes, bioimaging reagents and phototherapeutics. *Inorg. Chem. Front.* **2021**, *8*, 4553−4579.
(34) Jiang, K.; Sun, S.; Zhang, L.; Lu, Y.; Wu, A.; Cai, C.; Lin, H. Red, green, and blue luminescence by carbon dots: full-color emission tuning and multicolor cellular imaging. *Angew. Chem.* **2015**, *127*, 5450−5453.
(35) Lang, P.; Yeow, K.; Nichols, A.; Scheer, A. Cellular imaging in drug discovery. *Nat. Rev. Drug Discovery* **2006**, *5*, 343−356.
(36) Coelho-Cerqueira, E.; Pinheiro, A. S.; Follmer, C. Pitfalls associated with the use of Thioflavin-T to monitor anti-fibrillogenic activity. *Bioorg. Med. Chem. Lett.* **2014**, *24*, 3194−3198.
(37) Islam, A.; Kikuchi, Y.; Iimori, T. Electroabsorption and Stark Fluorescence Spectroscopies of Thioflavin T. *J. Phys. Chem. A* **2023**, *127*, 1436−1444.
(38) Ziaunys, M.; Smirnovas, V. Additional thioflavin-T binding mode in insulin fibril inner core region. *J. Phys. Chem. B* **2019**, *123*, 8727−8732.
(39) Amdursky, N.; Erez, Y.; Huppert, D. Molecular rotors: what lies behind the high sensitivity of the thioflavin-T fluorescent marker. *Acc. Chem. Res.* **2012**, *45*, 1548−1557.
(40) Kumar, P.; Nagarajan, A.; Uchil, P. D. Analysis of Cell Viability by the MTT Assay. *Cold Spring Harb Protoc.* **2018**, *2018* (6), 469−471.
(41) Njoki, P. N.; Lim, I. I. S.; Mott, D.; Park, H.-Y.; Khan, B.; Mishra, S.; Sujakumar, R.; Luo, J.; Zhong, C.-J. Size Correlation of Optical and Spectroscopic Properties for Gold Nanoparticles. *J. Phys. Chem. C* **2007**, *111*, 14664−14669.
(42) Liu, X.; Atwater, M.; Wang, J.; Huo, Q. Extinction coefficient of gold nanoparticles with different sizes and different capping ligands. *Colloids Surf., B* **2007**, *58*, 3−7.
(43) Maity, D.; Bhatt, M.; Paul, P. Calix[4]arene functionalized gold nanoparticles for colorimetric and bare-eye detection of iodide in aqueous media and periodate aided enhancement in sensitivity. *Microchim. Acta* **2015**, *182*, 377−384.
(44) Shrestha, S.; Wang, B.; Dutta, P. Nanoparticle processing: Understanding and controlling aggregation. *Adv. Colloid Interface Sci.* **2020**, *279*, 102162.
(45) Gayathry, T. C.; Gaur, M.; Mishra, L.; Mishra, M.; Barooah, N.; Bhasikuttan, A. C.; Mohanty, J. Supramolecular assembly of coumarin 7 with sulfobutylether-*β*-cyclodextrin for biomolecular applications. *Front. Chem.* **2023**, *11*, 1245518.
(46) Wang, F.; Wang, Y.-C.; Dou, S.; Xiong, M.-H.; Sun, T.-M.; Wang, J. Doxorubicin-tethered responsive gold nanoparticles facilitate intracellular drug delivery for overcoming multidrug resistance in cancer cells. *ACS Nano* **2011**, *5*, 3679−3692.
(47) Mihanfar, A.; Targhazeh, N.; Sadighparvar, S.; Darband, S. G.; Majidinia, M.; Yousefi, B. Doxorubicin loaded magnetism nanoparticles based on cyclodextrin dendritic-graphene oxide inhibited MCF-7 cell proliferation. *Bio. Mol. Concepts* **2021**, *12*, 8−15.
(48) Abd-Elhakeem, M. A.; Abdel-Haseb, O. M.; Abdel-Ghany, S. E.; Cevik, E.; Sabit, H. Doxorubicin loaded on chitosan-protamine nanoparticles triggers apoptosis via downregulating Bcl-2 in breast cancer cells. *J. Drug Delivery Sci. Technol.* **2020**, *55*, 101423.
(49) Butterworth, R. F. Potential for the Repurposing of Adamantane Antivirals for COVID-19. *Drugs in R&D* **2021**, *21*, 267−272.
(50) Dhawa, T.; Hazra, A.; Barma, A.; Pal, K.; Karmakar, P.; Roy, P. 4-Methyl-2,6-diformylphenol based biocompatible chemosensors for pH: discrimination between normal cells and cancer cells. *RSC Adv.* **2020**, *10*, 15501−15513.
(51) Fan, J.; Feng, Z.; Chen, N. Spermidine as a target for cancer therapy. *Pharmacol. Res.* **2020**, *159*, 104943.
(52) Son, S.; Kim, J.; Kim, J.; Kim, B.; Lee, J.; Kim, Y.; Li, M.; Kang, H.; Kim, J. S. Cancer therapeutics based on diverse energy sources. *Chem. Soc. Rev.* **2022**, *51*, 8201−8215.
(53) Chen, J.; Zhang, Y.; Zhao, L.; Zhang, Y.; Chen, L.; Ma, M.; Du, X.; Meng, Z.; Li, C.; Meng, Q. Supramolecular Drug Delivery System from Macrocycle-Based Self-Assembled Amphiphiles for Effective Tumor Therapy. *ACS Appl. Mater. Interfaces* **2021**, *13*, 53564−53573.
(54) Barooah, N.; Kunwar, A.; Khurana, R.; Bhasikuttan, A. C.; Mohanty, J. Stimuli-Responsive Cucurbit[7]uril-Mediated BSA Nanoassembly for Uptake and Release of Doxorubicin. *Chem.Asian J.* **2017**, *12*, 122−129.
(55) Stsiapura, V. I.; Maskevich, A. A.; Kuzmitsky, V. A.; Uversky, V. N.; Kuznetsova, I. M.; Turoverov, K. K. Thioflavin T as a Molecular Rotor: Fluorescent Properties of Thioflavin T in Solvents with Different Viscosity. *J. Phys. Chem. B* **2008**, *112*, 15893−15902.

https://doi.org/10.1021/acsphyschemau.4c00027
ACS Phys. Chem Au 2024, 4, 522−530